Contrib Mineral Petrol
DOI 10.1007/s00410-009-0374-9

ORIGINAL PAPER

C2/c pyroxene phenocrysts from three potassic series in the Neogene alkaline volcanics, NE Turkey: their crystal chemistry with petrogenetic significance as an indicator of *P–T* conditions

Faruk Aydin · Richard M. Thompson · Orhan Karsli · Hinako Uchida · Jason B. Burt · Robert T. Downs

Received: 19 August 2008 / Accepted: 5 January 2009

Abstract Chemical and structural data are reported for *C2/c* pyroxene phenocrysts collected from three potassic series (Group A: basanite-tephrite, Group B: tephrite-phonolitic tephrite, Group C: alkaline basalt-trachybasalt) of the Neogene alkaline volcanics (NAVs) in northeastern Turkey, in order to investigate the evolution of the magmatic plumbing system and the location of magma chamber(s) with crystallization conditions. The rock series hosting the clinopyroxene phenocrysts show generally porphyritic texture and have a variable phenocryst-rich nature (20–58%), with phenocryst assemblages characterized by cpx ± ol ± plag ± foid ± amp ± bio. The clinopyroxene phenocrysts can be chemically classified as Ti- and Fe^{3+}-rich Al-diopsides for Groups A and B (AB-cpxs) and Ti- and Fe^{3+}-poor Al-diopsides for Group C (C-cpxs). They have poorly variable composition, clustering in the diopside field. Structurally, the diopside groups have nearly similar *a* (ranging from 9.73 to 9.75 Å), V_{cell} (437.2–440.9 $Å^3$), and ⟨*beta*⟩ angle values (106.01°–106.23°), but some differences in polyhedral parameters and geometries of the AB-cpxs and C-cpxs have been observed. For example, the AB-cpxs are characterized by larger *c* (5.27–5.30 vs. 5.25–5.28 Å), V_T (2.27–2.30 vs. 2.23–2.28 $Å^3$), and V_{M2} (25.53–25.72 vs. 25.41–25.59 $Å^3$) values and smaller *b* (8.87–8.88 vs. 8.88–8.91 Å) and V_{M1} (11.49–11.63 vs. 11.64–11.83 $Å^3$) values with respect to the C-cpxs. In addition, the AB-cpxs show higher values of V_{M2}/V_{M1} (2.20–2.23) due to large V_{M2} and small V_{M1} compared to the V_{M2}/V_{M1} ratios of the C-cpxs (<2.19). Such differences in the crystal structure of the AB-cpxs and C-cpxs from the NAVs are partly related to different crystallization pressures, but mostly related to variation in melt composition and, possibly, the influence of other crystallizing mineral phases. In particular, R(M2-O1) and R(M1-O2) (i.e. bond lengths) differences in the clinopyroxenes of different groups support the presence of evolved host rocks with different alkaline character (i.e. silica-undersaturated Groups A–B and silica-saturated Group C). Based on the cpx-geothermobarometry, the crystallization pressures for the C-cpxs are lower than 4.5 kbars, but the AB-cpxs have relatively high-pressure values (5.6–10.6 kbars), suggesting that the AB-cpxs crystallized in higher pressure environments. The relatively higher crystallization temperatures of the AB-cpxs also indicate higher cooling rates. The *P–T* estimates suggest that the source regions of the clinopyroxene phenocrysts from the NAVs were crustal magma chambers in a closed plumbing system at a moderate- to low-pressure regime.

Keywords Clinopyroxene · Crystal-chemistry · Low pressure · Alkaline · Volcanics · NE Turkey

Communicated by G. Moore.

F. Aydin (✉)
Department of Geological Engineering, Nigde University, 51200 Nigde, Turkey
e-mail: faydin@nigde.edu.tr; faydin61@gmail.com

R. M. Thompson · H. Uchida · J. B. Burt · R. T. Downs
Department of Geosciences, University of Arizona, Tucson, AZ 85721-0077, USA

O. Karsli
Department of Geological Engineering, Gumushane University, 29000 Gumushane, Turkey

Introduction

Ca-rich clinopyroxene (*C2/c*) is one of the most common ferromagnesian minerals in alkaline potassic and sodic

Published online: 29 January 2009

rocks from various tectonic settings, and has been used as a petrogenetic indicator for distinct magmatic series. Crystal-chemical studies on clinopyroxenes have provided useful information on the origin of parental magmas and petrological evolution of host rocks (e.g. Bindi et al. 1999; Avanzinelli et al. 2004). In particular, structural and chemical diversities of clinopyroxenes have been interpreted to be the result of the different magma compositions (Cundari and Salviulo 1987; Dal Negro et al. 1989; Cellai et al. 1994; Pasqual et al. 1995; Bindi et al. 2002; Princivalle et al. 2000; Nazzareni et al. 2001) and/or physical conditions of crystallization (Dal Negro et al. 1982, 1989; Molin and Zanazzi 1991; Malgarotto et al. 1993; Nimis et al. 1996; Nimis 1998; Nazzareni et al. 1998). Some experimental studies showed that reliable information on crystallization temperatures and pressures of clinopyroxenes in compositionally similar rocks can be obtained (e.g. Molin and Zanazzi 1991; Nimis 1995, 1999; Nimis and Ulmer 1998).

In light of this, a detailed literature review related to the crystal-chemistry of clinopyroxenes from one of our research areas, the Neogene Alkaline volcanic series (NAVs) in the northeastern Turkey, has been performed. There have been several studies on the compositions and zoning types of the clinopyroxenes in the eastern part of the NAVs (e.g. Sen et al. 1998; Aydin 2003; Aydin et al. 2008a, b). There have been no studies on the structural characteristics of the clinopyroxenes in the NAVs in the literature. Therefore, the crystal structures for twelve diopside samples from these rocks have been refined, and the petrological interpretive techniques described above have been applied to them. The purpose of this paper is to fill this gap in our knowledge of this part of the world.

This study, based on high-quality crystal chemical data for *C2/c* pyroxene phenocrysts in the NAVs of northeastern Turkey, will:

1. evaluate the similarities and differences in the crystal chemistry of the clinopyroxene phenocrysts,
2. introduce the magmatic plumbing system and the location of magma chamber(s) in relation to crystallization conditions,
3. explain the origin and evolutionary history of the alkaline volcanism,
4. constitute a scientific basis for future petrological work in the region.

Geological setting and petrological outlines

The eastern Pontides of Turkey (northeastern Turkey), which form the eastern extension of the Pontides (Fig. 1), represent a very well-preserved magmatic arc system resulting from northward subduction of the northern branch of Neo-Tethyan oceanic crust beneath the Eurasian plate during Late Cretaceous (e.g. Sengör and Yilmaz 1981; Sengör et al. 1985; Okay 1989; Robinson et al. 1995; Yilmaz et al. 1997; Okay and Sahintürk 1997). The Eurasian plate collided with the Tauride–Anatolide platform in the north of Arabian platform (Fig. 1) in Late

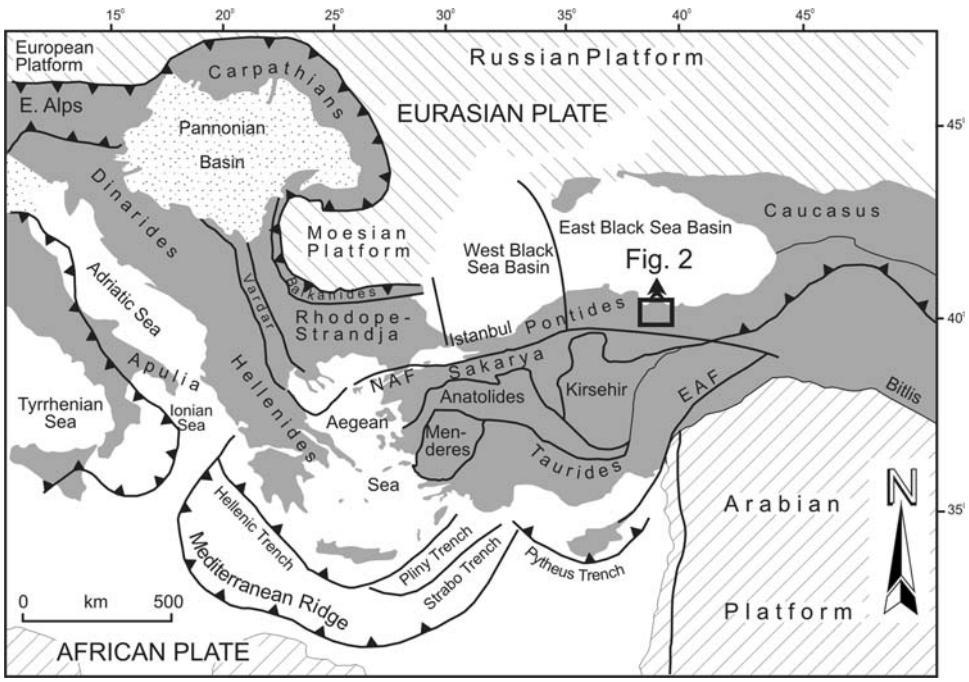

Fig. 1 Regional tectonic setting of Turkey in relation to the Afro-Arabian and Eurasian plates based on Dinter (1998) and Robertson (2000). *NAF* North Anatolian Fault, *EAF* East Anatolian Fault. Figure 2 indicates location of the study area

Palaeocene-Early Eocene time (e.g. Yilmaz et al. 1997; Keskin 2003; Sengör et al. 2003), and the ongoing convergence of these plates after their amalgamation led to continued compression of the eastern Pontides during the Oligocene to Early Miocene (e.g. Boztug et al. 2004, 2006; Keskin et al. 2008). This event resulted in the formation of the North Anatolian Fault (NAF in Fig. 1) in the Middle Miocene, allowing the westward escape of the Anatolian block (Sengör and Kidd 1979). The pressure release in the crust, due to the escape, triggered volcanism along major faults in the eastern Pontides during the Late Miocene to Pleistocene (Yilmaz et al. 2000; Yegingil et al. 2002; Boztug et al. 2004; Aydin et al. 2008a). In this regard, the eastern Pontides (NE-Turkey) recorded a complex history of subduction-, collision- and extension-related magmatic episodes from early/late Cretaceous to late Neogene.

The neotectonic framework of northeastern Turkey was shaped in Neogene-Quaternary time (Bozkurt 2001; Bozkurt and Mittwede 2001) by interactions between the Arabian and Eurasian plates (Fig. 1). During the neotectonic period, this activity produced a complex set of subduction zones from Greece to Iran, forming several volcanic provinces of different ages and compositions. Some important volcanic provinces in Turkey formed during this period (Fig. 2a), which are (1) Western Anatolian Volcanic Province (WAVP), (2) Central Anatolian Volcanic Province (CAVP), (3) Galatian Volcanic Province (GVP), (4) Eastern Anatolian Volcanic Province (EAVP), and (5) Northeastern Anatolian Volcanic Province (NEAVP). The NEAVP is a considerable part of the eastern Pontides (Fig. 2a, b), including Mesozoic-Cenozoic plutonic and volcanic rocks (Sen et al. 1998;

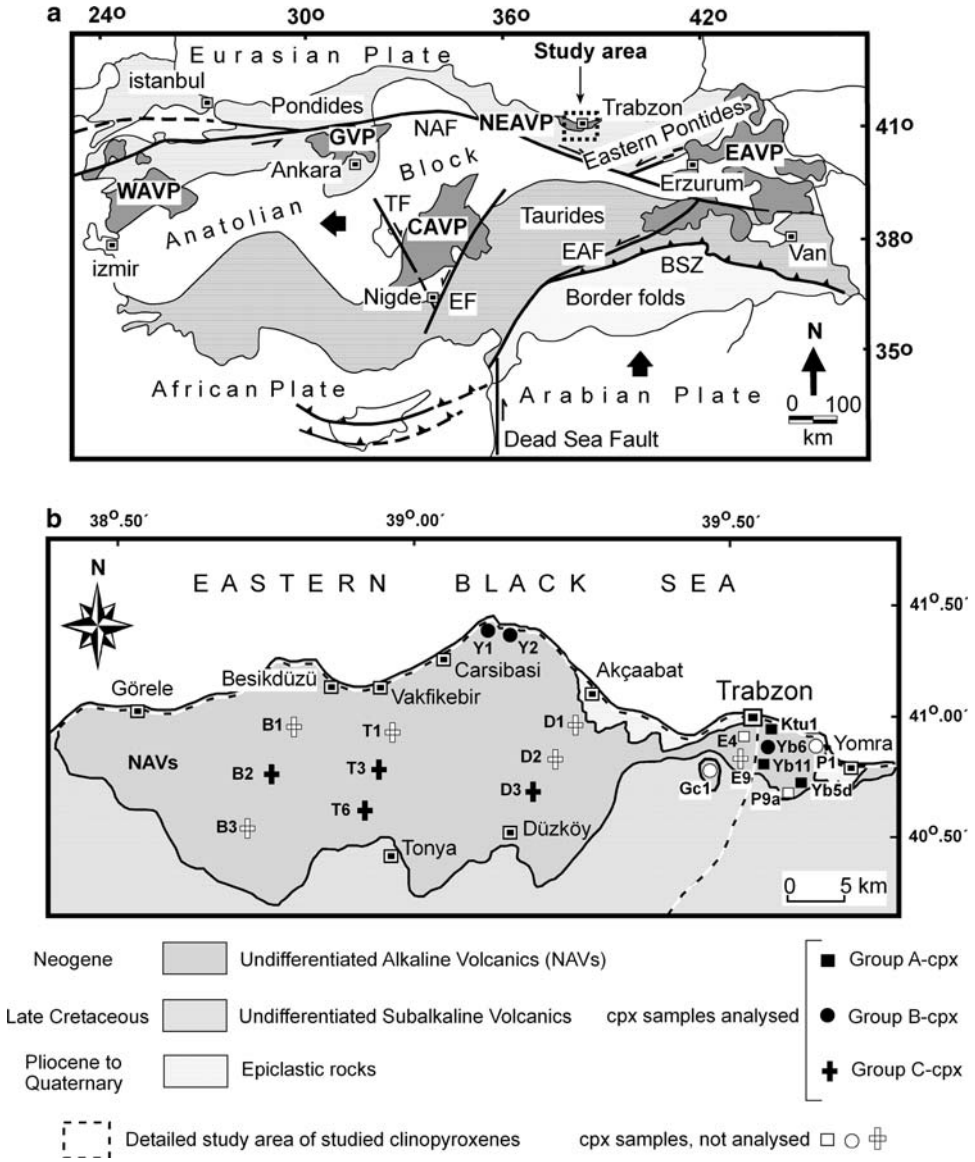

Fig. 2 **a** Simplified tectonic map of Turkey (modified after Sengör et al. 1985; Bozkurt 2001) showing distribution of Neo-Quaternary volcanic provinces (from Aydin et al. 2008b) with location of the alkaline volcanics hosting clinopyroxenes, **b** Simplified geological map of the northeastern alkaline volcanic province (NEAVP) and surrounding areas (after Güven 1993; Sen et al. 1998) with sample locations of the studied clinopyroxenes

Karsli et al. 2002, 2004a, b, 2007; Aydin et al. 2003, 2008a, b; Topuz et al. 2005; Boztug et al. 2006, 2007), and it is one of the most interesting provinces due to the presence of silica-undersaturated to silica-saturated potassic alkaline volcanic rocks hosting clinopyroxene phenocrysts.

Neogene alkaline volcanics (NAVs) cut Late Cretaceous subalkaline volcaniclastics and are widely exposed in the NEAVP, and they are covered by Pliocene-Quaternary epiclastic rocks (Fig. 2b). Radiometric ages showed that the alkaline volcanism occurred between early Miocene and late Pliocene times (Hoskin and Wysoczanski 1998; Barbieri et al. 2000; Aydin 2003). A detailed petrographic study of the NAVs, consisting of three different series [feldspar-free (Group A), feldspar and feldspathoid-bearing (Group B) and feldspathoid-free rocks (Group C)], was reported by Aydin et al. (2008a). A simple description of the rocks hosting the clinopyroxene samples that form the basis of this study is given in Table 1 and is summarized below.

The Neogene volcanics display generally porphyritic texture and have a variable phenocryst-rich nature (20–58%), with phenocryst assemblages characterized by clinopyroxene ± olivine ± plagioclase ± feldspathoid ± amphibole ± biotite. Clinopyroxene phenocrysts are mostly euhedral-subhedral shaped and range between 10 and 20 mm in size. They sometimes show oscillatory and sectorial zoning with Mg# [Mg/(Mg + Fe^t)] of 0.69–0.83. Olivine (Fo_{91-83}), amphibole (Mg# = 0.71 − 0.75) and biotite (Mg# = 0.71 − 0.84) have Mg-rich compositions. Feldspathoid minerals include sodalite, analcite and leucite, and they are found in the Groups A and B series. However, Ca-poor (An_{25-40}) and Ca-rich plagioclase feldspars (An_{51-70}) are only present in the Groups B and C. Apatite and Fe–Ti oxides are the most important accessory minerals of each series of the NAVs.

Geochemical and isotopic analyses of the NAVs have also been given in detail by Aydin et al. (2008a). The authors have suggested that elemental and isotopic (Nd–Sr–Pb) compositions for each series of the NAVs are very similar, and the source of alkaline magmas was derived from a young and homogeneous lithospheric mantle (T_{DM} = 0.51–0.59 Ga) enriched by an earlier subduction event. According to Aydin et al. (2008b), the alkaline magma hosting clinopyroxenes was therefore subject to a relatively low-pressure fractionation in closed-magma chambers at different levels by means of variations in the crystallization conditions during rapid ascent of the magma, resulting from post-collision extensional tectonic regime affecting the eastern Pontides during Middle Miocene-Pliocene.

Data collection and refinement

Twelve unzoned clinopyroxene crystals selected from four Group A, four Group B and three Group C rock series of the NAVs, northeastern Turkey, were analyzed for composition and structure. The sample compositions were analyzed on a Cameca SX50 Electron Microprobe at the University of Arizona. Operating conditions were: wavelength dispersive spectrometers, 15 kV accelerating voltage, and 20 nA beam current. Beam size for these analyses was 1 μm. Fe^{3+} contents of the clinopyroxenes were calculated stoichiometrically according to equation of Droop (1987). Single-crystal X-ray diffraction intensities were collected with a Bruker X8 APEX2 CCD X-ray diffractometer equipped with graphite-monochromator using MoKα radiation (λ = 0.71069 Å). The unit cell refinement and data reduction were preformed with the SAINT software (Bruker 2005). The structure was refined with SHELXL (Sheldrick 1997) using starting coordinates from Thompson and Downs (2008). Data collection and refinement statistics are in Table 2. Cell parameters and polyhedral geometry are given in Table 3. M2 was refined as a split position because single position refinements for M2 left an unacceptably large residual peak in close proximity to M2. All atoms were refined with anisotropic displacement parameters except for M2′, which was refined with fixed U_{iso} of 0.01 $Å^2$. The scattering curve for Ca was used for M2, Mg for M2′. M1 was refined with mixed Fe and Mg occupancy. M1 and M2 + M2′ occupancies were constrained to equal 1, except for sample T6. Sample T6 was Ca-deficient in comparison to the other samples, and refined best using mixed Fe and Mg occupancy for M2′. Sample T6 occupancies for M2 + M2′ were not constrained, but refined to equal 1 within error. Table 4 contains the chemical analyses and elemental cation partition among T, M1 and M2 sites. Atomic proportions were estimated on the basis of four cations. Table 5 lists final site occupancy assignments based on consideration of both microprobe and refinement results. Mn was arbitrarily assigned to M2′ in Table 5. Generalized chemical formulas of the samples in each series of the NAVs are clearly presented as follows:

Group A: Y*b*5d: $(Ca_{0.94}Na_{0.03}Mg_{0.02}Mn_{0.01})$
$(Mg_{0.72}Fe^{3+}_{0.13}Fe^{2+}_{0.07}Al_{0.04}Ti^{4+}_{0.04})(Si_{0.89}Al_{0.11})O_6$

Yb11: $(Ca_{0.94}Na_{0.04}\quad Mg_{0.01}Mn_{0.01})$
$(Mg_{0.65}Fe^{3+}_{0.19}Fe^{2+}_{0.04}Al_{0.05}Ti^{4+}_{0.07})(Si_{0.83}Al_{0.17})O_6$

Ktu1: $(Ca_{0.93}Na_{0.04}Mg_{0.02}Fe^{2+}_{0.01})$
$(Mg_{0.58}Fe^{3+}_{0.24}Al_{0.12}Ti^{4+}_{0.06})(Si_{0.81}Al_{0.19})O_6$

Table 1 General petrographical characteristics of the different rock series hosting clinopyroxenes

Rock series	Clinopyroxene sample no.	Rock name	Rock type	Texture	Phenocrysts-microphenocrysts modal ratios (%)	All crystals (%)	Groundmass (%)
Group A (feldspar-free series)	Yb5d	ol-tephrite	Pyroclastic	Vitrophyric	cpx (20) + soda + an (15) + ol (8) + ap (2) + Fe–Ti (3)	48	Glassy (52)
	Yb11	ol-tephrite	Lava	Porphyritic	cpx (22) + soda + an (13) + ol (6) + ap (2) + Fe–Ti (2)	45	Microcrystalline (55)
	Ktu1	ol-tephrite	Lava	Porphyritic	cpx (20) + soda + an (10) + ol (4) + ap (1) + Fe–Ti (1)	36	Microcrystalline (64)
	P9a	basanite	Pyroclastic	Porphyritic, trachytic	cpx (25) + soda + an (15) + ol (10) + ap (2) + Fe–Ti (3)	55	Microcrystalline (45)
	E4	basanite	Pyroclastic	Glomeroporphyritic	cpx (23) + soda + an (10) + ol (10) + ap (1) + Fe–Ti (2)	46	Microcrystalline (54)
Group B (feldspar and feldspathoid-bearing series)	Yb6	tephrite	Pyroclastic	Seriate, glomeroporphyritic	cpx (18) + soda + an (13) + pl (7) + sa (5) + ol (3) + bio (1) + ap (1) + Fe–Ti (2)	50	Microporphyritic (50)
	Y1	tephrite	lava	Porphyritic, glomeroporphyritic	cpx (20) + soda + an (15) + pl (10) + sa (5) + ol (3) + bio (2), ap (1), Fe–Ti (2)	58	Microcrystalline (42)
	Y2	tephrite	lava	Porphyritic, glomeroporphyritic	cpx (18) + soda + an (12) + pl (8) + sa (4) + ol (2) + bio (1) + ap (1) + Fe–Ti (2)	48	Microcrystalline (52)
	P1	tephrite	lava	Seriate, glomeroporphyritic	cpx (15) + soda + an (8) + pl (5) + sa (2) + bio (1) + ap (1) + Fe–Ti (2)	34	Microporphyritic (66)
	Gc1	tephrite	sill	Seriate, glomeroporphyritic	cpx (16) + soda + an (10) + pl (6) + sa (3) + bio (2) + ap (1) + Fe–Ti (2)	40	Microporphyritic (60)
Group C (feldspathoid-free series)	D1	ol-alkaline basalt	lava	Porphyritic	cpx (25) + pl (10) + ol (5) + ap (1) + Fe–Ti (3)	44	Microcrystalline (56)
	D2	trachy- basalt	lava	Microlitic-porphyritic	cpx (23) + pl (7) + sa (2) + bio (1) + amp (1) + ap (1), Fe–Ti (3)	38	Microcrystalline (62)
	D3	ol-alkaline basalt	pyroclastic	Microlitic-porphyritic	cpx (25) + pl (10) + ol (5) + bio (3) + amp (2) + ap (2) + Fe–Ti (3)	50	Microcrystalline (50)
	T1	alkaline basalt	lava	Porphyritic	cpx (20) + pl (8) + sa (2) + ol (2) + ap (1) + Fe–Ti (1)	36	Microcrystalline (64)
	T3	alkaline basalt	pyroclastic	Porphyritic	cpx (18) + pl (7) + sa (2) + ol (3) + ap (1) + Fe–Ti (1)	32	Microcrystalline (68)
	T6	alkaline basalt	pyroclastic	Porphyritic	cpx (15) + pl (9) + sa (1) + ol (3) + ap (1) + Fe–Ti (1)	30	Microcrystalline (70)
	B1	alkaline basalt	Lava	Microlitic-porphyritic	cpx (10) + pl (5) + sa (2) + bio (1) + ap (1) + Fe–Ti (1)	20	Microcrystalline (80)
	B2	trachy- basalt	Pyroclastic	Porphyritic, glomeroporphyritic	cpx (15) + pl (10) + sa (3) + bio (2) + ap (1) + Fe–Ti (3)	34	Microporphyritic (66)
	B3	alkaline basalt	Pyroclastic	Porphyritic	cpx (13) + pl (10) + sa (2) + bio (2) + ap (1), Fe–Ti (2)	30	Microcrystalline (70)
	E9	alkaline basalt	Sill	Porphyritic, glomeroporphyritic	cpx (25) + pl (8)+ sa (4) + ol (3) + bio (2) + ap (1) + Fe–Ti (2)	45	Microporphyritic (55)

cpx clinopyroxene, *soda* sodalite, *an* analcite, *ol* olivine, *amp* amphibole, *bio* biotite, *pl* plagioclase, *sa* sanidine, *ap* apatite, *Fe–Ti* Fe–Ti oxide

The locations of all cpx-samples (analysed and not analysed) are indicated in Fig. 2b. Modal abundances of all samples were determined by counting about 800 points. Phenocrysts–microphenocrysts range from 20 to 5 mm

Group B: Y6*b*: $(Ca_{0.89}Na_{0.05}Mg_{0.04}Fe^{2+}_{0.01}Mn_{0.01})$
$(Mg_{0.71}Fe^{3+}_{0.14}Fe^{2+}_{0.07}Al_{0.05}Ti^{4+}_{0.03})(Si_{0.90}Al_{0.10})O_6$
Y1: $(Ca_{0.92}Na_{0.04}Mg_{0.02}Fe^{2+}_{0.01}Mn_{0.01})$
$(Mg_{0.68}Fe^{3+}_{0.14}Fe^{2+}_{0.07}Al_{0.08}Ti^{4+}_{0.03})(Si_{0.88}Al_{0.12})O_6$
Y2: $(Ca_{0.92}Na_{0.04}Mg_{0.02}Fe^{2+}_{0.01}Mn_{0.01})$
$(Mg_{0.67}Fe^{3+}_{0.17}Fe^{2+}_{0.05}Al_{0.07}Ti^{4+}_{0.04})(Si_{0.86}Al_{0.14})O_6$
P1: $(Ca_{0.95}Na_{0.03}Mg_{0.02})(Mg_{0.70}Fe^{3+}_{0.15}Fe^{2+}_{0.03}Al_{0.08}Ti^{4+}_{0.04})$
$(Si_{0.86}Al_{0.14})O_6$

Group C: D3: $(Ca_{0.89}Na_{0.02}Mg_{0.06}Fe^{2+}_{0.02}Mn_{0.01})$
$(Mg_{0.82}Fe^{3+}_{0.08}Fe^{2+}_{0.06}Al_{0.02}Ti^{4+}_{0.01}Cr_{0.01})(Si_{0.95}Al_{0.05})O_6$
T3: $(Ca_{0.92}Na_{0.02}Mg_{0.04}Fe^{2+}_{0.02})$
$(Mg_{0.69}Fe^{3+}_{0.13}Fe^{2+}_{0.08}Al_{0.05}Ti^{4+}_{0.05})(Si_{0.87}Al_{0.13})O_6$
T6: $(Ca_{0.82}Na_{0.03}Mg_{0.10}Fe^{2+}_{0.04}Mn_{0.01})$
$(Mg_{0.69}Fe^{3+}_{0.05}Fe^{2+}_{0.19}Al_{0.04}Ti^{4+}_{0.03})(Si_{0.94}Al_{0.06})O_6$
B2: $(Ca_{0.86}Na_{0.03}Mg_{0.07}Fe^{2+}_{0.03}Mn_{0.01})$
$(Mg_{0.73}Fe^{3+}_{0.10}Fe^{2+}_{0.12}Al_{0.03}Ti^{4+}_{0.02})(Si_{0.93}Al_{0.07})O_6$
E9: $(Ca_{.093}Na_{0.03}Mg_{0.03}Fe^{2+}_{0.01})$
$(Mg_{0.79}Fe^{3+}_{0.11}Fe^{2+}_{0.04}Al_{0.04}Ti^{4+}_{0.02})(Si_{0.92}Al_{0.08})O_6$

Results

Crystal chemistry

Structural parameters and chemical compositions of the investigated *C2/c* pyroxene phenocrysts are presented in Tables 2, 3, 4 and 5. In the conventional classification diagram (Morimoto 1989), the clinopyroxenes of each series (Groups A, B and C) from the NAVs have nearly similar chemical compositions (Fig. 3). All clinopyroxenes are diopsidic in composition, and most of them fall within the illustrated lower (Wo_{45}) and upper (Wo_{50}) boundaries, but some compositions (particularly Groups A and B) plot above the 50% Ca line in the pyroxene quadrilateral, as a result of high contents of non-quadrilateral components (i.e. Fe^{3+}-rich). Consequently, their compositions vary from Ti- and Fe^{3+}-rich Al-diopsides (Groups A and B diopsides) to Ti- and Fe^{3+}-poor ones (Group C diopsides). Groups A and B diopsides (AB-cpxs) have higher contents of Ti (0.04–0.07 a.f.u.), Al^{vi} (0.04–0.11 a.f.u.) and Fe^{3+} contents (0.13–0.19 a.f.u.) with respect to Group C diopsides (C-cpxs). The latter has lower contents of Ti (mostly <0.04 a.f.u.), Al (mostly <0.04 a.f.u.) and Fe^{3+} (<0.12 a.f.u.) (Table 4).

Cell parameters

In the studied clinopyroxenes, *a* (9.73–9.75 Å) and unit cell volume, V_{cell}, (437.2–440.9 Å^3) values are rather similar (Table 3) and do not show a good correlation with rock group. However, the AB-cpxs are characterized by higher c (5.27–5.30 Å), V_T (2.27–2.30 Å^3), and V_{M2} (25.53–25.72 Å^3) values, and lower *b* (8.87–8.88 Å) and V_{M1} (11.49–11.63 Å^3) values with respect to the C-cpxs. The latter has lower values of *c* (5.25–5.28 Å), V_T (2.23–2.28 Å^3), and V_{M2} (25.41–25.59 Å^3), and higher values of *b* (8.88–8.91 Å) and V_{M1} (11.64–11.83 Å^3) (Table 3). The difference in the range of variation of *c* values reflects their distinct Al^{IV} contents (Al^{IV} = 0.04–0.11 for AB-cpxs and 0.01–0.05 for C-cpxs). The ⟨*beta*⟩ angles of all the clinopyroxenes are generally similar (106.0°–106.2°) and are not negatively correlated with V_{cell} (Fig. 4).

T polyhedron

In all of the clinopyroxenes, microprobe analysis shows that there is sufficient Al to compensate for Si deficiencies in the tetrahedral site (T site) without requiring any tetrahedral iron. The T site in the AB-cpxs is characterized by relatively high Al^{IV} content (0.20–0.39 a.f.u.), compared to that of the C-cpxs (0.11–0.25 a.f.u.). The C-cpxs have relatively lower Al_{total} (0.12–.030 a.f.u.), whereas the AB-cpxs have higher values (Al_{total} = 0.26–0.51 a.f.u.). In Fig. 5a, the proportion of Al in the tetrahedron (Al_t) is plotted versus the proportion of trivalent cations, R^{3+}, in the M1 site.

M1 polyhedron

The M1 site is dominated by Mg (0.57–0.82 a.f.u.) with minor amounts of Fe^{2+} (0.05–0.14 a.f.u.) and variable contents of R^{3+} (Fe^{3+} + Ti^{4+} + Al^{3+} + Cr^{3+} = 0.12–0.37 a.f.u.). This substitution mechanism causes significant variation in the M1–O bond lengths (⟨M1–O⟩ = 2.057–2.076 Å) and in the polyhedral volumes (V_{M1} = 11.49–11.83 Å^3). The shortening of the M1-O2 bond length is well correlated with the increase of R^{3+} content as documented by Dal Negro et al. (1982). In Fig. 5b, the C-cpxs can clearly be distinguished from those of the AB-cpxs by their longer M1-O2 bond lengths (2.022–2.044 Å and 2.008–2.022 Å, respectively).

M2 polyhedron

The M2 site is essentially filled by Ca + Na (0.84–0.98 a.f.u.) in all of the clinopyroxenes. The volume of the M2 polyhedron (V_{M2}) ranges from 25.41 to 25.72 Å^3 (Table 3) and generally increases with (Ca + Na) content (Fig. 5c).

Table 2 Data collection and refinement statistics for the studied clinopyroxene phenocrysts in space group *C2/c*

Rock series	Group A			Group B				Group C				
Sample	Yb5d	Yb11	Ktu1	Y6b	Y1	Y2	P1	D3	T3	T6	B2	E9
Measured reflections	7196	9752	9009	9985	10631	7595	10470	8092	7650	10358	8320	9162
Unique reflections	1758	2428	2011	2181	2095	1678	2484	1848	1708	2148	1758	1819
Refl. with $I > 2\sigma(I)$	1546	1948	1727	1911	1811	1473	2052	1624	1316	1641	1624	1533
R_{int}	0.017	0.022	0.020	0.019	0.017	0.020	0.022	0.021	0.033	0.032	0.016	0.024
θ_{max} (°)	45.3	52.4	48.8	50.9	48.8	45.2	56.3	45.5	44.0	48.7	45.3	48.8
$R[F^2 > 2\sigma(F^2)]$	0.021	0.028	0.021	0.021	0.021	0.024	0.023	0.022	0.029	0.030	0.022	0.023
$wR(F^2)$	0.055	0.072	0.060	0.062	0.058	0.059	0.060	0.062	0.070	0.077	0.061	0.059
S	1.11	1.10	1.10	1.11	1.11	1.10	1.10	1.11	1.04	1.08	1.10	1.09
Parameters	51	51	51	51	51	51	51	51	51	53	51	51
a_w*	0.024	0.0343	0.029	0.0288	0.0244	0.0233	0.0262	0.0239	0.0311	0.0324	0.0261	0.022
b_w*	0.3006	0.0862	0.1473	0.2514	0.3122	0.455	0.1259	0.4867	0.2485	0.2595	0.5711	0.3919
$(\Delta/\sigma)_{max}$	3.191	5.217	2.255	2.645	3.602	3.347	2.524	0.001	2.173	1.740	0.001	0.001
$\Delta\rho_{max}$ (e Å^{-3})	0.48	0.98	0.46	0.99	0.99	0.66	0.59	1.22	0.63	1.08	1.64	0.56
$\Delta\rho_{min}$ (e Å^{-3})	−0.45	−0.51	−0.41	−0.45	−0.49	−0.48	−0.49	−0.62	−0.55	−0.62	−0.64	−0.53
Extinction coefficient	0.0000 (9)	0.000 (1)	0.000 (1)	0.000 (1)	0.0000 (9)	0.0000 (9)	0.0000 (9)	0.019 (1)	0.000 (1)	0.000 (1)	0.003 (1)	0.005 (1)

* $w = 1/[\sigma^2(F_o^2) + (a_wP)^2 + b_wP]$, $P = (F_o^2 + 2F_c^2)/3$, $Fc^* = kFc[1 + 0.001 \times Fc^2\lambda^3/\sin(2\theta)]^{-1/4}$

The AB-cpxs have relatively higher (Ca + Na) contents (0.94–0.98 a.f.u.) whereas the C-cpxs are characterized by lower (Ca + Na) contents (0.84–0.96 a.f.u.), with Fe, Mg and Mn bringing the M2 site to full occupancy. Decreasing the (Ca + Na) content corresponds to increasing the (Fe^{2+} + Mg + Mn) sum in the M2. M2 is a split site, with (Fe^{2+} + Mg + Mn) going into M2′. R(M2′-O3) is quite long, and (Fe^{2+} + Mg + Mn) in the M2′ site are probably coordinated only to O1 and O2 (Bindi et al. 1999).

Some crystallographic parameters and their relationships with the chemistry of the clinopyroxenes are presented below in terms of site geometry and occupancies.

Compositional and structural variations

Compositional variations in the octahedral M1 site of the studied clinopyroxenes are shown in Fig. 6a–d, in which cation abundances are plotted against the Mg_{M1} of the clinopyroxenes. In these figures, Mg_{M1} shows a negative correlation with Fe^{3+}, Al^{3+}, R^{3+} and Ti^{4+}. This indicates the substitution vectors characterizing the clinopyroxene phenocrysts. The higher values of Mg_{M1} characterize the Group C-cpxs of the NAVs, whereas relatively lower values are observed for the Group AB-cpxs. By considering the range of Mg_{M1} values of the clinopyroxenes, the C-cpxs mostly fall in a well-separated field relative to the AB-cpxs (Fig. 6a–d). Consequently, these cation variations in the octahedral M1 site alter significantly the M1 volume (V_{M1}) as well as the other polyhedral parameters such as bond lengths, and V_{M2}/V_{M1}.

More structural modifications associated with cation substitution are shown in Fig. 7 [$\langle beta \rangle$ angle vs. (V_{M2}/V_{M1})]. The AB-cpxs show higher values of V_{M2}/V_{M1} (2.20–2.23), due to large V_{M2} (25.5–25.7 Å^3) and small V_{M1} (11.5–11.6 Å), related to high Ca + Na (0.94–0.98 a.f.u.) and R^{3+} contents (0.22–0.37 a.f.u.) whereas the C-cpxs show lower V_{M2}/V_{M1} ratios (<2.19), due to their lower Ca + Na (mostly <0.94 a.f.u.) and R^{3+} contents (<0.22 a.f.u.). Some clinopyroxenes (T3, T6 and B2 crystals) in the Group C show relatively high values of $\langle beta \rangle$ angle due to higher Fe^{2+} contents (Table 4).

Figure 8, illustrating the relationship between the site occupancy of M1 and M2, plots R(M2-O1) versus R(M1-O2), comparing the clinopyroxenes in this study with *C2/c* pyroxenes from alkaline undersaturated rocks of the Monte Vulture Volcano (Bindi et al. 1999) and calcalkaline/alkaline lavas of the Stromboli–Alicudi–Vulcano (S–A–V) volcanoes (Pasqual et al. 1995; Nazzareni et al. 1998; Faraone et al. 1988) in Italy. The data from the studied clinopyroxenes show clear and regular variations, overlapping the fields of *C2/c* pyroxene from alkaline undersaturated rocks of the Monte Vulture Volcano in Italy. The Group AB-cpxs of the feldspathoid-bearing rocks from the NAVs have shorter M1-O2 (<2.022 Å) and longer M2-O1 (>2.370 Å) distances (Table 3; Fig. 8), with respect to those of feldspar-bearing (feldspathoid-free)

Table 3 Cell parameters and polyhedral geometry for the clinopyroxene phenocrysts from different rock series

Rock series	Group A			Group B				Group C				
Sample	Yb5d	Yb11	Ktu1	Y6b	Y1	Y2	P1	D3	T3	T6	B2	E9
a (Å)	9.7533 (4)	9.7455 (3)	9.7425 (3)	9.7357 (3)	9.7391 (3)	9.7318 (3)	9.7274 (4)	9.7367 (3)	9.7433 (3)	9.7325 (4)	9.7375 (6)	9.7344 (3)
b (Å)	8.8833 (3)	8.8657 (3)	8.8644 (3)	8.8774 (3)	8.8835 (3)	8.8771 (3)	8.8648 (3)	8.9088 (3)	8.8808 (3)	8.9004 (3)	8.8976 (6)	8.8927 (3)
c (Å)	5.2938 (2)	5.2870 (2)	5.2955 (2)	5.2818 (2)	5.2835 (2)	5.2770 (1)	5.2744 (2)	5.2513 (2)	5.2820 (2)	5.2641 (2)	5.2705 (3)	5.2629 (1)
β (°)	106.010 (2)	106.034 (2)	106.006 (1)	106.058 (1)	106.022 (2)	106.047 (2)	106.013 (2)	106.015 (2)	106.087 (2)	106.225 (2)	106.170 (3)	106.013 (2)
V (Å^3)	440.87 (3)	439.03 (3)	439.60 (3)	438.68 (3)	439.36 (3)	438.12 (2)	437.17 (3)	437.83 (3)	439.15 (3)	437.83 (5)	438.57 (5)	437.91 (2)
T site												
T-O1	1.6274 (6)	1.6275 (6)	1.6314 (6)	1.6220 (5)	1.6220 (6)	1.6200 (7)	1.6210 (5)	1.6048 (6)	1.6231 (9)	1.6115 (8)	1.6149 (6)	1.6116 (7)
T-O2	1.6101 (6)	1.6103 (6)	1.6147 (6)	1.6054 (5)	1.6045 (6)	1.6035 (7)	1.6039 (5)	1.5903 (6)	1.6064 (9)	1.5972 (7)	1.5980 (6)	1.5954 (7)
T-O3, A1	1.6751 (6)	1.6723 (5)	1.6758 (5)	1.6707 (5)	1.6713 (5)	1.6698 (6)	1.6703 (5)	1.6651 (6)	1.6711 (8)	1.6636 (7)	1.6670 (6)	1.6680 (6)
T-O3, A2	1.6962 (6)	1.6918 (6)	1.6951 (5)	1.6897 (5)	1.6910 (5)	1.6890 (7)	1.6899 (5)	1.6839 (6)	1.6922 (9)	1.6834 (7)	1.6864 (6)	1.6858 (6)
Mean	1.6522	1.6505	1.6543	1.6470	1.6472	1.6456	1.6463	1.6360	1.6482	1.6389	1.6416	1.6402
V(T) (Å^3)	2.30	2.29	2.30	2.27	2.27	2.27	2.27	2.23	2.28	2.24	2.25	2.25
M(1) site												
M1-O1, A1	2.1217 (6)	2.1212 (6)	2.1175 (5)	2.1214 (5)	2.1211 (5)	2.1192 (7)	2.1151 (5)	2.1248 (6)	2.1217 (8)	2.1308 (7)	2.1285 (6)	2.1209 (6)
M1-O1, A2	2.0517 (6)	2.0486 (6)	2.0459 (5)	2.0509 (5)	2.0522 (5)	2.0502 (6)	2.0458 (5)	2.0583 (6)	2.0524 (8)	2.0581 (7)	2.0563 (6)	2.0532 (6)
M1-O2	2.0189 (6)	2.0122 (6)	2.0085 (6)	2.0182 (5)	2.0217 (6)	2.0204 (7)	2.0175 (5)	2.0440 (6)	2.0221 (9)	2.0347 (7)	2.0327 (6)	2.0331 (7)
Mean	2.0641	2.0607	2.0573	2.0635	2.0650	2.0633	2.0595	2.0757	2.0654	2.0745	2.0725	2.0691
V(M1) (Å^3)	11.61	11.55	11.49	11.61	11.63	11.60	11.54	11.83	11.64	11.81	11.77	11.71
M(2) site												
M2-O1	2.3801 (6)	2.3762 (6)	2.3800 (6)	2.3714 (6)	2.3711 (6)	2.3699 (8)	2.3714 (6)	2.3588 (7)	2.367 (1)	2.363 (1)	2.3614 (7)	2.3659 (7)
M2-O2	2.3613 (6)	2.3568 (6)	2.3641 (5)	2.3501 (5)	2.3513 (6)	2.3475 (7)	2.3520 (5)	2.3269 (7)	2.3419 (9)	2.3113 (9)	2.3261 (7)	2.3400 (7)
M2-O3, C1	2.5450 (7)	2.5420 (7)	2.540 (1)	2.5466 (6)	2.5491 (7)	2.5474 (8)	2.5415 (6)	2.5619 (7)	2.551 (1)	2.557 (1)	2.5591 (8)	2.5523 (8)
M2-O3, C2	2.6923 (6)	2.6885 (6)	2.6827 (9)	2.6990 (6)	2.7013 (6)	2.6990 (8)	2.6900 (6)	2.7182 (7)	2.7002 (9)	2.715 (1)	2.7131 (7)	2.7093 (7)
Mean	2.4947	2.4909	2.4917	2.4918	2.4932	2.4910	2.4887	2.4915	2.4900	2.4866	2.4899	2.4919
V(M2) (Å^3)	25.72	25.62	25.64	25.61	25.65	25.58	25.53	25.55	25.55	25.41	25.53	25.59
M(2′) site												
M2′-O1	2.22 (1)	2.15 (1)	2.22 (2)	2.091 (9)	2.09 (1)	2.09 (2)	2.12 (1)	2.06 (1)	2.07 (1)	2.103 (5)	2.071 (7)	2.08 (1)
M2′-O2	2.326 (2)	2.312 (2)	2.328 (2)	2.3012 (9)	2.303 (1)	2.299 (2)	2.305 (2)	2.2827 (8)	2.292 (1)	2.2676 (9)	2.2800 (8)	2.294 (1)
O3-O3-O3	165.80	165.70	165.76	165.80	165.73	165.82	165.87	165.73	165.55	165.24	165.38	165.98

Cell parameters and polyhedral geometry are obtained by single crystal X-ray diffraction method. *a*, *b*, *c* and ⟨*beta*⟩ *angle* (*β*); Unit cell parameters, *V* volume of unit cell

Table 4 Chemical compositions, elemental cation partition among T, M1 and M2 sites, and end-members for the clinopyroxene phenocrysts from different rock series

Rock series	Group A						Group B								Group C									
Sample	Yb5d		Yb11		Ktu1		Yb6		Y1		Y2		P1		D3		T3		T6		B2		E9	
	avg	stdev	avg	stdev	avg	stdev	avg	stdev	avg	stdev	avg	stdev	avg	stdev	avg	stdev	avg	stdev	avg	stdev	avg	stdev	avg	stdev
SiO_2	47.94	0.93	44.40	1.11	42.96	0.39	48.59	0.57	47.40	0.64	46.29	0.36	46.28	0.50	51.41	1.42	46.95	1.67	50.53	0.48	49.80	0.71	49.48	0.95
TiO_2	1.28	0.16	2.44	0.31	2.21	0.06	1.16	0.16	1.21	0.07	1.55	0.11	1.27	0.08	0.39	0.15	1.90	0.51	0.88	0.11	0.82	0.12	0.86	0.13
Al_2O_3	5.81	0.92	8.66	0.69	11.46	0.28	5.90	0.54	7.07	0.60	7.67	0.29	8.21	0.32	2.84	1.11	6.91	1.22	3.61	0.49	3.85	0.55	4.84	0.86
Cr_2O_3	0.01	0.01	0.01	0.01	0.00	0.01	0.02	0.02	0.01	0.01	0.02	0.02	0.09	0.08	0.42	0.21	0.05	0.04	0.01	0.01	0.05	0.03	0.12	0.03
FeO	6.86	0.35	7.93	0.43	8.14	0.10	7.24	0.28	7.26	0.21	7.58	0.14	6.19	0.34	5.53	1.16	7.26	1.21	9.38	0.35	8.12	0.32	5.13	0.76
MnO	0.16	0.02	0.15	0.03	0.14	0.02	0.20	0.02	0.21	0.02	0.18	0.03	0.08	0.02	0.15	0.03	0.14	0.05	0.29	0.02	0.23	0.01	0.08	0.03
MgO	13.32	0.40	11.80	0.42	10.55	0.17	13.54	0.39	12.65	0.36	12.41	0.15	12.97	0.31	16.05	0.83	13.06	0.98	14.36	0.27	14.46	0.32	14.68	0.75
CaO	23.67	0.17	23.35	0.15	23.28	0.08	22.53	0.22	22.95	0.12	22.93	0.11	23.90	0.15	22.69	0.50	23.01	0.47	20.46	0.32	21.61	0.15	23.52	0.19
Na_2O	0.45	0.04	0.51	0.05	0.56	0.04	0.65	0.05	0.54	0.05	0.57	0.03	0.39	0.06	0.26	0.04	0.31	0.08	0.35	0.03	0.36	0.01	0.40	0.09
Sum	99.52		99.26		99.31		99.83		99.33		99.22		99.40		99.76		99.60		99.87		99.31		99.12	
T-site																								
Si	1.780	0.032	1.663	0.036	1.609	0.012	1.796	0.018	1.765	0.019	1.728	0.011	1.716	0.015	1.889	0.039	1.748	0.051	1.880	0.016	1.856	0.025	1.832	0.030
Al^{iv}	0.220	0.032	0.337	0.036	0.391	0.012	0.204	0.018	0.235	0.019	0.272	0.011	0.284	0.015	0.111	0.039	0.252	0.051	0.120	0.016	0.144	0.025	0.168	0.030
Sum	2.000		2.000		2.000		2.000		2.000		2.000		2.000		2.000		2.000		2.000		2.000		2.000	
M1-site																								
Mg	0.724	0.022	0.644	0.021	0.577	0.008	0.714	0.020	0.682	0.019	0.668	0.008	0.701	0.017	0.824	0.040	0.696	0.050	0.735	0.014	0.751	0.018	0.786	0.039
Fe^{2+}	0.059	0.015	0.050	0.018	0.054	0.012	0.068	0.009	0.079	0.016	0.061	0.010	0.023	0.019	0.057	0.022	0.083	0.042	0.143	0.013	0.101	0.014	0.042	0.013
Al^{vi}	0.035	0.012	0.045	0.009	0.114	0.005	0.053	0.011	0.076	0.015	0.065	0.008	0.075	0.010	0.012	0.014	0.051	0.012	0.038	0.009	0.025	0.005	0.043	0.010
Fe^{3+}	0.146	0.021	0.192	0.028	0.193	0.013	0.133	0.011	0.129	0.018	0.162	0.013	0.166	0.018	0.084	0.029	0.117	0.031	0.059	0.013	0.100	0.021	0.105	0.024
Cr	0.000	0.000	0.000	0.000	0.000	0.000	0.000	0.000	0.000	0.000	0.000	0.000	0.000	0.000	0.012	0.006	0.000	0.000	0.000	0.000	0.000	0.000	0.000	0.000
Ti	0.036	0.005	0.069	0.009	0.062	0.002	0.032	0.005	0.034	0.002	0.044	0.003	0.035	0.002	0.011	0.004	0.053	0.015	0.025	0.003	0.023	0.003	0.024	0.004
Sum	1.000		1.000		1.000		1.000		1.000		1.000		1.000		1.000		1.000		1.000		1.000		1.000	
M2-site																								
Ca	0.942	0.006	0.937	0.005	0.935	0.003	0.892	0.009	0.915	0.006	0.916	0.004	0.950	0.007	0.892	0.014	0.918	0.015	0.816	0.013	0.862	0.007	0.933	0.006
Na	0.032	0.003	0.037	0.003	0.040	0.003	0.047	0.004	0.039	0.004	0.042	0.002	0.028	0.004	0.019	0.003	0.022	0.006	0.025	0.003	0.026	0.001	0.028	0.006
Mg	0.013		0.014		0.013		0.032		0.021		0.022		0.016		0.055		0.030		0.060		0.052		0.026	
Fe^{2+}	0.008		0.007		0.008		0.023		0.018		0.014		0.004		0.029		0.026		0.090		0.053		0.010	
Mn	0.005	0.001	0.005	0.001	0.004	0.001	0.006	0.001	0.007	0.001	0.006	0.001	0.002	0.001	0.005	0.001	0.004	0.001	0.009	0.001	0.007	0.000	0.003	0.001
Sum	1.000		1.000		1.000		1.000		1.000		1.000		1.000		1.000		1.000		1.000		1.000		1.000	
R^{3+}	0.216		0.305		0.370		0.219		0.240		0.270		0.277		0.119		0.222		0.121		0.148		0.175	
Mg#	0.77		0.72		0.69		0.76		0.75		0.74		0.79		0.83		0.76		0.73		0.76		0.83	
Wo	48.81		49.68		51.26		46.58		48.44		48.44		50.29		45.42		48.42		42.11		44.21		48.29	
En	38.19		34.94		32.33		38.96		37.18		36.50		37.96		44.71		38.24		41.07		41.14		41.93	
Fs	11.35		13.41		14.22		12.01		12.32		12.84		10.27		8.90		12.18		15.53		13.32		8.33	
Ac	1.65		1.97		2.19		2.45		2.06		2.22		1.48		0.97		1.16		1.29		1.33		1.45	

Major element compositions of the clinopyroxenes in wt % are obtained by electron microprobe. Structural formulae calculated on the basis of six oxygens. Mg# = (Mg/Mg + Fe^t), Fe^t= Fe^{2+} + Fe^{3+} + Mn, R^{3+} = (Al^{vi} + Fe^{3+} + Cr^{3+} + Ti^{4+}), and partitioning of Fe^{2+} and Mg at M1 and M2, respectively, were done according to Dal Negro et al. (1982)

Table 5 Final site occupancy assignments for the clinopyroxene phenocrysts from different rock series

Rock series	Sample	M2	M2′	M1	*T*
Group A	Yb5d	$0.94Ca + 0.03Na$	$0.02Mg + 0.01Mn$	$0.72Mg + 0.13Fe^{3+} + 0.07Fe^{2+} + 0.04Al + 0.04Ti^{4+}$	$0.89Si + 0.11Al$
	Yb11	$0.94Ca + 0.04Na$	$0.01Mg + 0.01Mn$	$0.65Mg + 0.19Fe^{3+} + 0.04Fe^{2+} + 0.05Al + 0.07Ti^{4+}$	$0.83Si + 0.17Al$
	Ktu1	$0.93Ca + 0.04Na$	$0.02Mg + 0.01Fe^{2+}$	$0.58Mg + 0.24Fe^{3+} + 0.12Al + 0.06Ti^{4+}$	$0.81Si + 0.19Al$
Group B	Y6b	$0.89Ca + 0.05Na$	$0.04Mg + 0.01Fe^{2+} + 0.01Mn$	$0.71Mg + 0.14Fe^{3+} + 0.07Fe^{2+} + 0.05Al + 0.03Ti^{4+}$	$0.90Si + 0.10Al$
	Y1	$0.92Ca + 0.04Na$	$0.02Mg + 0.01Fe^{2+} + 0.01Mn$	$0.68Mg + 0.14Fe^{3+} + 0.07Fe^{2+} + 0.08Al + 0.03Ti^{4+}$	$0.88Si + 0.12Al$
	Y2	$0.92Ca + 0.04Na$	$0.02Mg + 0.01Fe^{2+} + 0.01Mn$	$0.67Mg + 0.17Fe^{3+} + 0.05Fe^{2+} + 0.07Al + 0.04Ti^{4+}$	$0.86Si + 0.14Al$
	P1	$0.95Ca + 0.03Na$	$0.02Mg$	$0.70Mg + 0.15Fe^{3+} + 0.03Fe^{2+} + 0.08Al + 0.04Ti^{4+}$	$0.86Si + 0.14Al$
Group C	D3	$0.89Ca + 0.02Na$	$0.06Mg + 0.02Fe^{2+} + 0.01Mn$	$0.82Mg + 0.08Fe^{3+} + 0.06Fe^{2+} + 0.02Al + 0.01Ti^{4+} + 0.01Cr$	$0.95Si + 0.05Al$
	T3	$0.92Ca + 0.02Na$	$0.04Mg + 0.02Fe^{2+}$	$0.69Mg + 0.13Fe^{3+} + 0.08Fe^{2+} + 0.05Al + 0.05Ti^{4+}$	$0.87Si + 0.13Al$
	T6	$0.82Ca + 0.03Na$	$0.10Mg + 0.04Fe^{2+} + 0.01Mn$	$0.69Mg + 0.05Fe^{3+} + 0.19Fe^{2+} + 0.04Al + 0.03Ti^{4+}$	$0.94Si + 0.06Al$
	B2	$0.86Ca + 0.03Na$	$0.07Mg + 0.03Fe^{2+} + 0.01Mn$	$0.73Mg + 0.10Fe^{3+} + 0.12Fe^{2+} + 0.03Al + 0.02Ti^{4+}$	$0.93Si + 0.07Al$
	E9	$0.93Ca + 0.03Na$	$0.03Mg + 0.01Fe^{2+}$	$0.79Mg + 0.11Fe^{3+} + 0.04Fe^{2+} + 0.04Al + 0.02Ti^{4+}$	$0.92Si + 0.08Al$

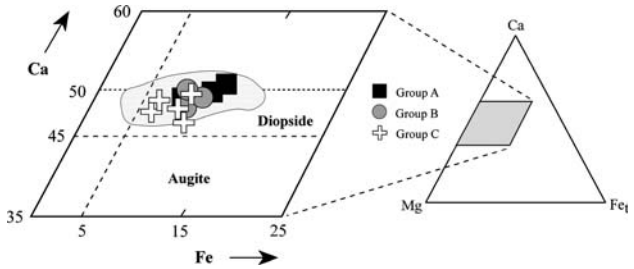

Fig. 3 Clinopyroxene compositions from the different rock series (Groups A, B and C) plotted in the Ca–Mg–Fe triangular diagram (Morimoto 1989). Shaded field, data sources: Aydin et al. (2008b)

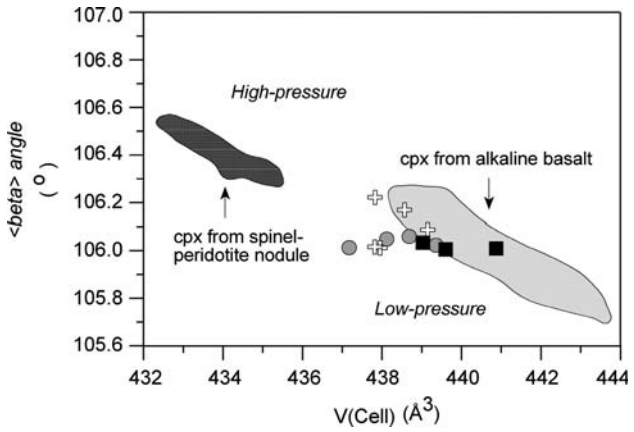

Fig. 4 V_{cell} versus $\langle beta \rangle$ angle. Data sources for comparison: high-pressure clinopyroxenes from spinel-peridotite nodules (Dal Negro et al. 1984), low-pressure clinopyroxenes from alkaline basalt (Dal Negro et al. 1989). *Symbols* are as in Fig. 3

Group A rocks. On the other hand, *C2/c* pyroxenes from the S–A–V volcanoes in Italy have strongly different bond lengths (M1-O2 = 2.037–2.042 Å and M2-O1 = 2.325–2.356 Å).

Geothermobarometry

The crystallization presssure of the clinopyroxene phenocrysts in this study has been estimated using the models developed by Nimis (1995, 1999, 2000) and Putirka et al. (1996, 2003). The model of Nimis estimates pressures using only structural parameters and/or compositions of clinopyroxenes. For the three potassic series of the NAVs, this results in low pressure values (4.6–1.5 kbars for Group AB-cpxs; 2.8–0.0 kbars for Group C-cpxs). As the pressures are calculated, model structural parameters such as V_{cell}, V_{M1} and V_{M2} are simultaneously created, and have been compared with those from the single-crystal XRD analyses. However, the pressures estimated by using Putirka's model, which are derived from the mineral-liquid equilibrium, are relatively higher than those from Nimis's approach (10.6–5.6 kbars for Group AB-cpxs; 4.5–3.0 kbars for Group C-cpxs). These pressures show clear variations between different series of the NAVs. All differences are presented in Table 6 and Fig. 9a. Additionally, the crystallization temperatures of the clinopyroxenes have been estimated using the mineral and host-rock compositions and their equilibrium conditions, as described by Putirka et al. (1996, 2003). These temperature results are presented in Table 6 and Fig. 9b.

In Figs. 9a and b, the pressures and temperatures of the clinopyroxenes have been plotted for the three potassic series of the NAVs. In Fig. 9a, the AB-cpxs (>5.6 kbars) can be clearly distinguished from the C-cpxs (<4.5 kbars) by taking into consideration their crystallization pressures. In Fig. 9b, the crystallization temperature values of the clinopyroxenes in the Groups A and B rock series mostly fall in the same range (mostly from 1,180 to 1,260°C) while the clinopyroxenes in the Group C series have largely low-temperature values (<1,170°C).

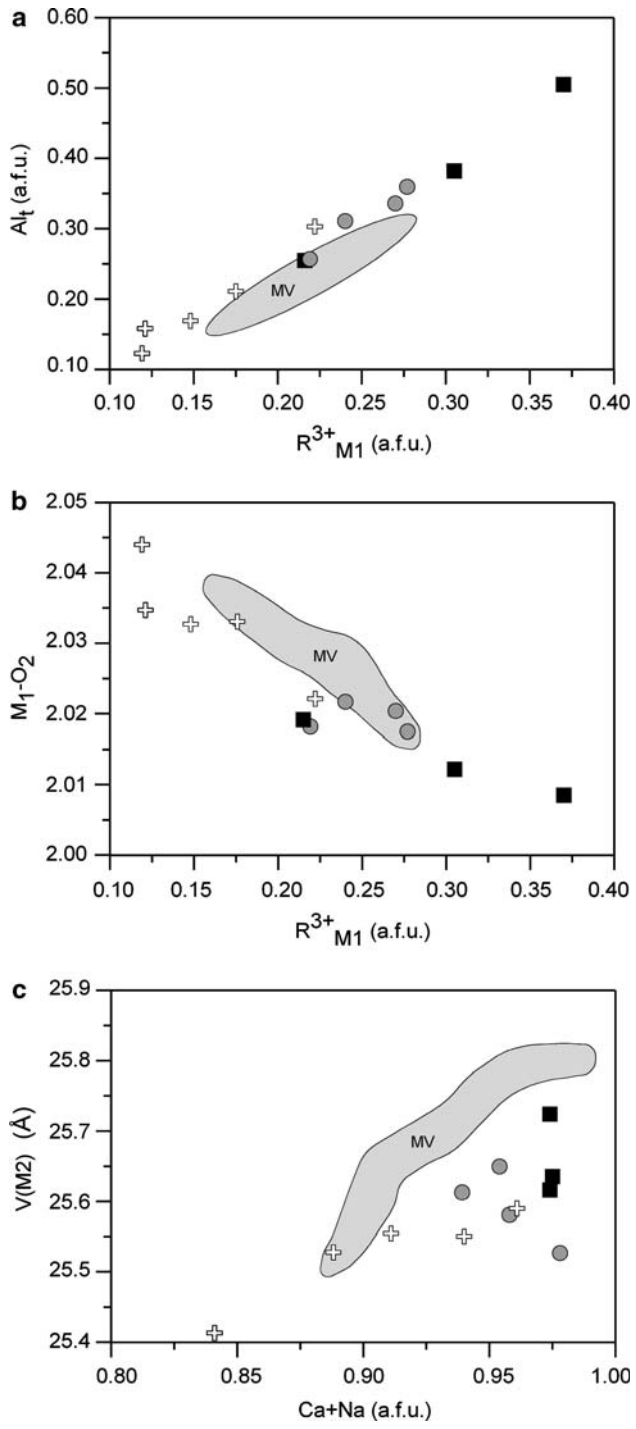

Fig. 5 **a** Plot of the R^{3+}_{M1} ($Fe^{3+} + Ti^{4+} + Al^{3+} + Cr^{3+}$) versus Al_t, **b** Relationship between M1-O2 bond length and R^{3+}_{M1}, **c** Plot of (Ca + Na) versus M2 polyhedron volumes (VM2). *Symbols* are as in Fig. 3. *Shaded field* clinopyroxenes from alkaline undersaturated rocks of the Monte Vulture Volcano (MV), Italy (Bindi et al. 1999). Note that the silica-saturated Group C rock series (alkaline basalt-trachybasalt) can be clearly distinguished from the silica-undersaturated Groups A (basanite-tephrite) and B (tephrite-phonolitic tephrite)

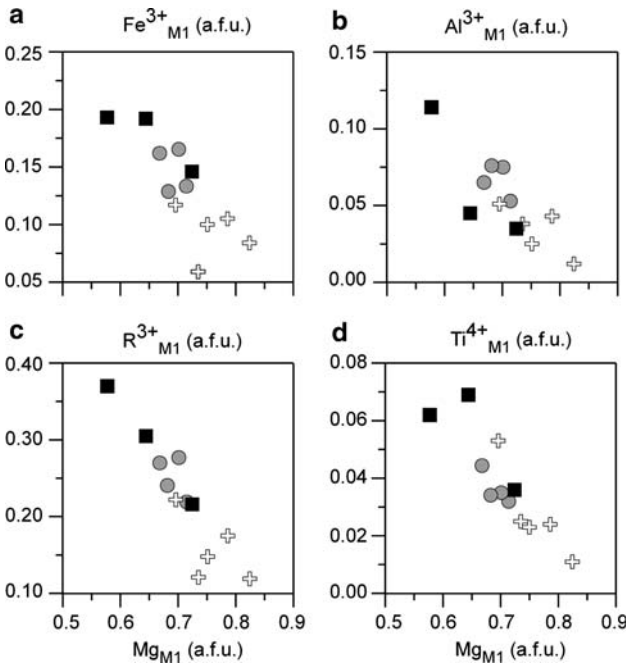

Fig. 6 Values of Mg# (Mg/Mg + Fe^t) for the studied clinopyroxenes against **a** Mg_{M1}, **b** Fe_{M1}^{2+}, **c** Al_{M1}^{3+}, **d** Fe_{M1}^{3+}, **e** R_{M1}^{3+} and **f** Ti_{M1}^{4+}

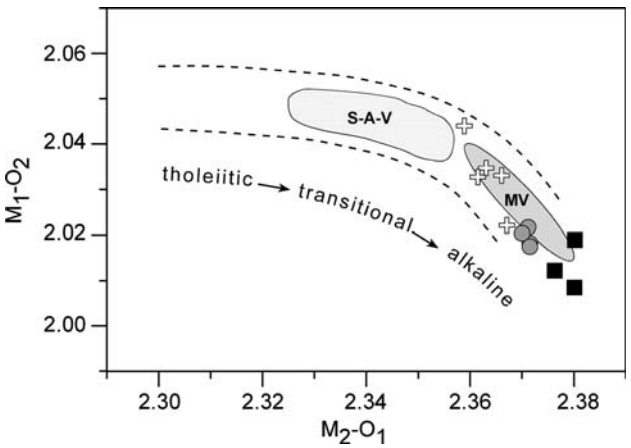

Fig. 7 Plot of M2-O1 versus M1-O2 bond lengths for the studied clinopyroxenes from the NAVs. *Symbols* are as in Fig. 3. Data sources for comparison: MV; clinopyroxenes from alkaline undersaturated rocks of the Monte Vulture Volcano (MV), Italy (Bindi et al. 1999), S–A–V; clinopyroxenes from transitional to alkaline volcanic rocks of the Stromboli (Pasqual et al. 1995), Alicudi (Nazzareni et al. 1998), and Vulcano (Faraone et al. 1988)

Discussion

The clinopyroxene phenocrysts were collected from the most mafic rocks (basanite, tephrite and alkaline basalt) of three different series (Groups A, B and C) of Neogene

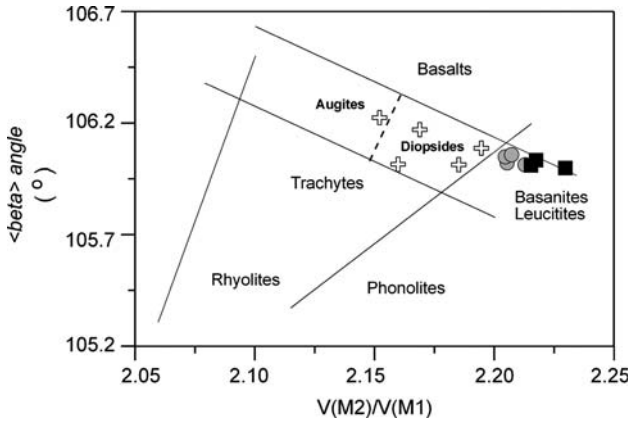

Fig. 8 Monoclinic ⟨*beta*⟩ angle versus volume ratio of M1 and M2 sites (VM2/VM1). *Dashed line* separates augites from diopsides (from Malgarotto et al. 1993). *Symbols* are as in Fig. 3

alkaline volcanics (NAVs), NE-Turkey. By taking into consideration the geochemical and isotopic data of the NAVs, it can be stated that the mafic rocks from different volcanic series hosting the clinopyroxene phenocrysts have basically similar chemical compositions (i.e. potassic character) even if they have different alkaline character (e.g. silica-undersaturated vs. silica-saturated). Also, it should be stressed that the source of their parent magma originated from a young and homogeneous lithospheric mantle (Aydin et al. 2008a). Moreover, it should be particularly emphasized that the alkaline magma derived from lithospheric mantle was exposed to a relatively low-pressure crystallization process in closed-magma chambers at different levels of the crust during differentiation and ascent of the magma (Aydin et al. 2008b). Therefore, the most mafic rocks of the NAVs are not a product of primary magma because they have undergone considerable low-pressure fractional crystallization, generating a wide variety of rock types with different degrees of evolution.

Based on the chemical and structural data of clinopyroxene phenocrysts from these mafic rocks of the NAVs, the studied clinopyroxenes have been classified as AB-cpxs (Ti- and Fe^{3+}-rich Al-diopsides in the Groups A and B series) and C-cpxs (Ti- and Fe^{3+}-poor Al-diopsides in the Group C series). Although these clinopyroxenes have similar *a*, V_{cell}, and ⟨*beta*⟩ angle values, limited variations in polyhedral size and geometry have been observed. For example, the AB-cpxs are characterized by higher *c*, V_T, V_{M2}, and R(M2-O1) and lower *b*, V_{M1}, and R(M1-O2) values with respect to the C-cpxs. A comparison of bond lengths and polyhedral volumes shows that the C-cpxs, with similar cell volumes and ⟨*beta*⟩ angle values to the AB-cpxs, generally have higher V_{M1} and R(M1-O2) (Fig. 10a), and lower V_{M2} and R(M2-O1) (Fig. 10b). Such differences between each group of clinopyroxenes in the R(M2-O1) versus R(M1-O2) diagram (Fig. 7) should be related to the origin and/or evolution of source magmas. In this study, taking into consideration of geochemical and isotopic data, some structural and chemical variations, observed in the clinopyroxene phenocrysts of the different volcanic series, can be mostly ascribed to the evolution process of the magma via relatively low-pressure fractionation rather than the origin or crystallization pressure.

The reason for the pressure differences obtained from the models of Nimis and Putirka, is probably "structural relaxation" en route to the surface. The crystallization temperature values of the Group AB-cpxs are mostly higher than those of the Group C-cpxs. In fact, this indicates a higher cooling rate (Dal Negro et al. 1982; Malgarotto et al. 1993) of the silica-undersaturated lavas (i.e. Groups A and B series).

As discussed by Dal Negro et al. (1989), V_{cell} is affected by pressure during crystallization, and M1 is the most pressure-sensitive polyhedral unit. In the studied clinopyroxenes, V_{cell} and V_{M1} values vary from 437 to 441 Å^3 and ~11.5 to 11.8 Å^3, respectively (Table 3; Fig. 11),

Table 6 Estimated pressures (*P*), depths (*D*) and temperatures (*T*) for clinopyroxene phenocrysts from different rock series of the NAVs

	Feldspar-free series (Group A)		Feldspar and feldspathoid-bearing series (Group B)		Feldspathoid-free series (Group C)	
Clinopyroxene sample no.	Yb5d, Yb11, Ktu1, P9a, E4		Yb6, Y1, Y2, P1, Gc1		D3, T3, T6, B2, E9	
Rock types	Basanite to tephrite		Tephrite to tephritic phonolite		Alkaline basalt to trachybasalt	
P (kbar)[a,b]	10.6–7.2[a]	4.6–1.5[b]	8.3–5.6[a]	4.6–1.2[b]	4.5–3.0[a]	2.8–0.0[b]
D (km)	32–22	14–4.5	25–17	14 – 3.6	13.5–9	8.4–0
T (°C)[a]	1,260–1,215		1,239–1,166		1,216–1,151	

1 kbar ≈ 3 km

[a] The pressures and the crystallization temperatures estimated from the thermometric approaches and equations are based on the studies of Putirka et al. (1996, 2003)

[b] The pressures are calculated according to Nimis (1995, 1999, 2000)

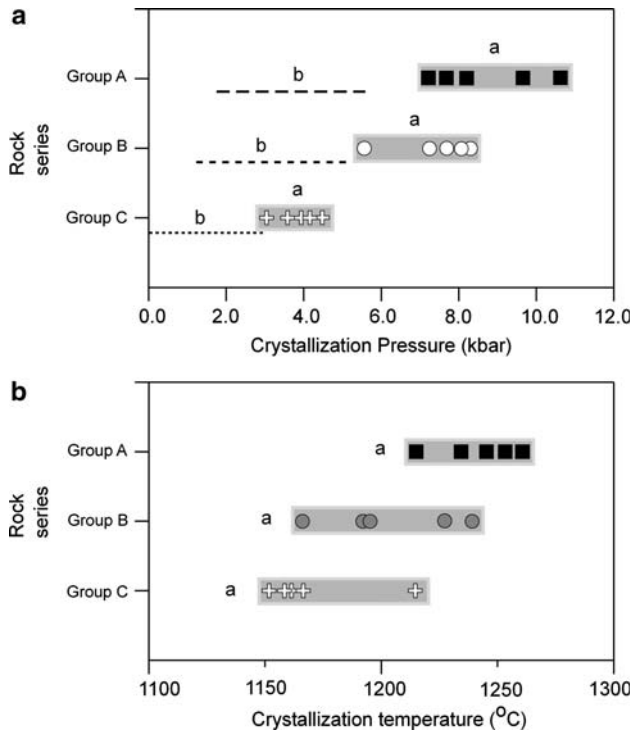

Fig. 9 **a** Crystallization pressures (kbar) of the studied clinopyroxene phenocrysts versus the rock series of NAVs. The pressures calculated according to (*a*) Putirka et al. (1996, 2003) and (*b*) Nimis (1995, 1999, 2000). **b** Crystallization temperatures (°C) of the studied clinopyroxene phenocrysts versus the rock series of NAVs. For the crystallization temperatures used the equations based on the works of (*a*) Putirka et al. (1996, 2003). *Symbols* are as in Fig. 3

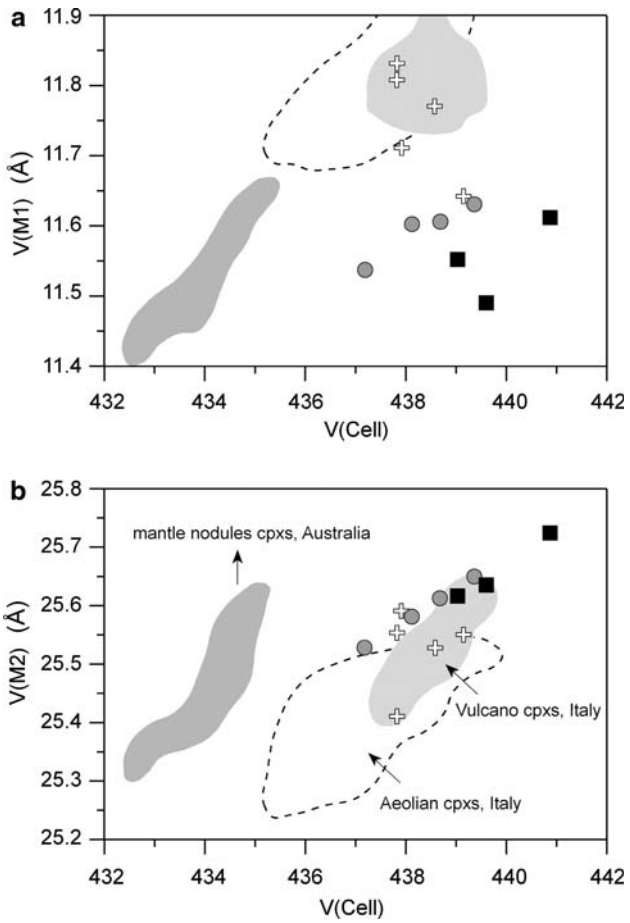

Fig. 10 **a** Cell volume (V_{cell}) versus M1 volume, **b** cell volume (V_{cell}) versus M2 volume. *Symbols* are as in Fig. 3. Data sources for comparison: Mantle nodule-clinopyroxenes from Victoria, Australia (Dal Negro et al. 1984); Vulcano and Aeolian clinopyroxenes from Italy (Faraone et al. 1988; Malgarotto et al. 1993, respectively)

suggesting relatively low-pressure conditions (<10 kbars). An estimate of crystallization pressure for near-liquidus *C2/c* pyroxenes has been proposed by Nimis (1995) on the basis of the V_{cell}–V_{M1} relationship. Figure 11 shows that the maximum pressure of clinopyroxene crystallization for the basic rocks of each series is about 7–8 kbars. The studied clinopyroxenes have higher V_{cell} and lower $\langle beta \rangle$ angle values than those of high-pressure clinopyroxenes ($V_{cell} < 436$ Å^3; $\langle beta \rangle$ angle >106.2°) from spinel peridotite (Dal Negro et al. 1984) whereas their V_{cell} (>438 Å^3) and $\langle beta \rangle$ angle (<106.2°) values are similar to low-pressure clinopyroxenes in alkaline basalts from Victoria, Australia (Dal Negro et al. 1989). These structural features are consistent with the mineral assemblages of the NAVs and with the values of pressure quantitatively calculated by Aydin et al. (2008a, b), supporting a relatively low-pressure regime for the genesis of the clinopyroxenes crystallizing in the crustal environment. The pressure values of the AB-cpxs (>7.0 kbars) estimated from this study (calculated by means of the model developed Putirka et al. 1996, 2003) are higher than those of the C-cpxs (∼ <5 kbars), indicating relatively higher crystallization pressure (Figs. 9a, 12).

V_{cell} versus polyhedral volumes of M1 and M2 are also reported in Fig. 10a and b; for comparison, low- to high-pressure clinopyroxenes data from Vulcano (Faraone et al. 1988) and Aeolian (Malgarotto et al. 1993) Islands, Italy, and mantle-nodule clinopyroxenes from Victoria, Australia (Dal Negro et al. 1984) are also included. The clinopyroxenes in this study generally show higher values of V_{cell} and V_{M2} than those of mantle clinopyroxenes. Higher pressure conditions for the Aeolian and Vulcano clinopyroxenes with larger V_{M1} can also be inferred from Fig. 10a. In sum, all these structural features indicate that the clinopyroxenes in this study cannot be xenoliths from rocks crystallized under high-pressure conditions or mantle environments.

P–T estimates for the clinopyroxenes in this study based on *C2/c* pyroxene geothermobarometry (Putirka et al. 1996, 2003; Nimis 1995, 1999, 2000) are shown in Fig. 12. Geotherms for several different geodynamic environments (Griffin et al. 1979; Jones et al. 1983; Takahashi and Kushiro 1983; Nimis 1998) and the location

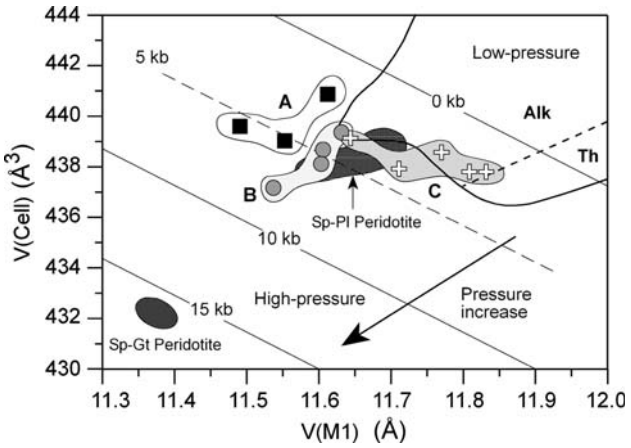

Fig. 11 Relationship between VM1 and *V*cell volumes of the studied clinopyroxene phenocrysts from the different rock series of NAVs (Groups A, B and C), and those for spinel-plagioclase (Sp-Pl) peridotite from Zabargard and spinel-garnet (Sp-Gt) peridotite from Tasmania (Nimis 1995). *Alk* Alkaline, *Th* Tholeiitic fields (Dal Negro et al. 1989). Geobarometric grids for basaltic systems are from Nimis (1995). *Symbols* are as in Fig. 3

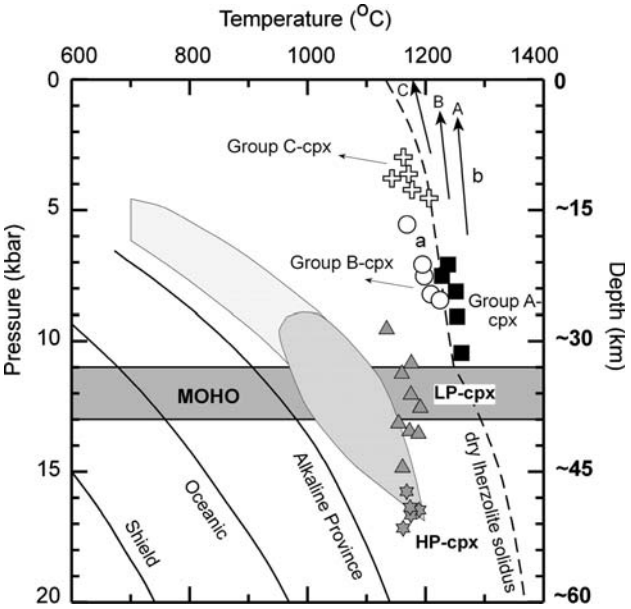

Fig. 12 Pressure–temperature (*P–T*) diagram to illustrate the potential source region for the *C2/c* pyroxene phenocrysts of the three potassic series (Groups A, B and C) based on the results of clinopyroxene-geobarometry (*a*) (Putirka et al. 1996, 2003; (*b*) Nimis 2000) and clinopyroxene-thermometry (Putirka et al. 1996, 2003). Dry peridotite solidus is after Takahashi and Kushiro (1983). The position of the Moho discontinuity is based on data from Cakir et al. (2000) and Cakir and Erduran (2004). Shaded and hatched fields represent the possible *P–T* fields for medium-grained and coarse-grained pyroxenites, respectively (Nimis 1998). Geotherms for alkaline province (Jones et al. 1983), shield and oceanic areas (Griffin et al. 1979) are shown for comparison. LP-cpx; low-pressure clinopyroxenes (*solid triangles*), HP-cpx; high-pressure clinopyroxenes (*solid stars*) are from Victoria, Australia (Dal Negro et al. 1989). Other symbols are as in Fig. 3

of the Moho discontinuity (Cakir et al. 2000; Cakir and Erduran 2004) are also shown. In addition, the studied clinopyroxenes are compared with high-pressure (HP-cpx) and low-pressure (LP-cpx) Ca-rich clinopyroxenes from alkaline basalts of Victoria in Australia (Dal Negro et al. 1989). *P–T* conditions for the geotherms in the different geodynamic environments and the Moho discontinuity in the study area do not match the studied clinopyroxenes. On the contrary, the crystal chemical characteristics of the clinopyroxenes result from *P–T* conditions typical of crustal magma chambers under moderate to low-pressure regimes.

Concluding remarks

In this study, the similarities and differences in the crystal chemistry of the clinopyroxenes from three potassic series of the NAVs from the eastern Pontides, NE-Turkey, have been evaluated, and the relationship of the petrological evolution of the clinopyroxenes to the crystallization conditions and the composition of the magma has been investigated. Based on the structural and compositional data of the clinopyroxenes, the following conclusions can be drawn:

1. Strong compositional and structural similarities between AB-cpxs and C-cpxs of the NAVs, NE-Turkey, indicate similar petrogenetic environments. Limited variations in the crystal chemistry of the clinopyroxenes are partly related to different crystallization pressures, but mostly reflect the variation in melt composition and, possibly, the influence of other crystallizing mineral phases. In particular, the differences of bond lengths, R(M2-O1) and R(M1-O2), between the different groups clinopyroxenes support the presence of the evolved magmas with different alkaline characters.
2. Based on the geobarometry of Putirka et al. (1996, 2003), the crystallization pressures of the clinopyroxenes in this study range from 3.0 to 10.6 kbars. In detail, the clinopyroxene phenocrysts from Group C series crystallized at pressures below 4.5 kbars, while the Group B-cpxs' crystallization pressures ranged from 5.6 to 8.3 kbars, and the Group A-cpxs crystallized at pressures from 7.2 to 10.6 kbars. Thus, it is clear that the pressure values of the AB-cpxs (mostly >7.0 kbars) are higher than those of the C-cpxs (<4.5 kbars), indicating relatively higher crystallization pressure. Consequently, it can be said that, in spite of these pressure differences, the crystallization and equilibration processes take place in a crustal environment at moderate to low depths.

3. According to the *P–T* diagram in this study and the geodynamic and petrogenetic models proposed by Aydin et al. (2008a, b), the parent magmas rose from lithospheric-mantle depths, reaching the upper part of the lower crust as crustal extension permitted the ascent of the magma. Successively, they have undergone considerable fractional crystallization of clinopyroxene with feldspathoid and/or feldspar minerals in a closed magmatic plumbing system, generating a wide variety of rock types. The estimated crystallization pressures and mineral assemblages of each potassic series from the NAVs have shown a good agreement with the evolution of the plumbing system suggested by Aydin et al. (2008b).
4. The crystallization temperatures range mostly from 1,180 to 1,260°C for the AB-cpxs, <1,170°C for C-cpxs. This indicates a higher cooling rate of the alkaline-rich lavas in the Groups A and B series of the NAVs.

Acknowledgments The authors are glad to thank the DAAD for the partial financial support. Many thanks are given to M. Burhan Sadiklar (Karadeniz Teknik University, Trabzon, Turkey) for logistic support. Moreover, they would like to give special thanks to Rainer Altherr and Hans-Peter Meyer (Mineralogisches Institut, Universität Heidelberg, Germany) for the electron microprobe analyses of some clinopyroxene phenocrysts. Thoughtful reviews made by Keith Putirka and anonymous peer-reviewers greatly improved the original manuscript. Editorial managing by Gordon Moore is really appreciated. We would like to thank the National Science Foundation for funding RMT, HU, and JAB through grants No. EAR-0622371 and No. EAR-0609906.

References

Avanzinelli R, Bindi L, Menchetti S, Conticelli S (2004) Crystallisation and genesis of peralkaline magmas from Pantelleria Volcano, Italy: an integrated petrological and crystal-chemical study. Lithos 73:41–69. doi:10.1016/j.lithos.2003.10.007

Aydin F (2003) Mineral chemistry, petrology and petrogenesis of the Degirmendere Valley volcanics (Trabzon–Esiroglu, NE-Turkey). PhD thesis. Karadeniz Technical University, Trabzon, Turkey (in Turkish with English abstract, unpublished)

Aydin F, Karsli O, Sadiklar MB (2003) Mineralogy and chemistry of biotites from eastern Pontide granitoid roks, NE Turkey: some petrological implications for granitoid magmas. Chem Erde-Geochem 63:163–182. doi:10.1078/0009-2819-00027

Aydin F, Karsli O, Chen B (2008a) Petrogenesis of the Neogene alkaline volcanics with implications for post-collisional lithospheric thinning of the Eastern Pontides, NE Turkey. Lithos 104:249–266. doi:10.1016/j.lithos.2007.12.010

Aydin F, Karsli O, Sadiklar MB (2008b) Compositional variations and zoning types of low-pressure clinopyroxenes in the Neogene alkaline volcanic rocks with petrogenetic implications, northeastern Turkey. Turk J Earth Sci (in press)

Barbieri M, Conforto L, Garbarino C, Masi U, Nicoletti M, Akinci Ö (2000) Geo-chemistry of hydrothermally-altered volcanic rocks of the upper volcanic cycle from the Eastern Pontides (Northeastern Turkey). Chem Erde-Geochem 60:81–95

Bindi L, Cellai D, Melluso L, Conticelli S, Morra V, Menchetti S (1999) Crystal chemistry of clinopyroxene from alkaline undersaturated rocks of the Monte Vulture Volcano, Italy. Lithos 46:259–274. doi:10.1016/S0024-4937(98)00069-3

Bindi L, Taselli F, Olmi F, Peccerillo A, Menchetti S (2002) Crystal chemistry of clinopyroxenes from Linosa Volcano, Sicily Channel, Italy: implications for modelling the magmatic plumbing system. Mineral Mag 66:953–968. doi:10.1180/0026461026660070

Bozkurt E (2001) Neotectonics of Turkey—a synthesis. Geodin Acta 14:3–30. doi:10.1016/S0985-3111(01)01066-X

Bozkurt E, Mittwede SK (2001) Introduction to the geology of Turkey—a synthesis. Int Geol Rev 43:578–594

Boztug D, Jonckheere R, Wagner GA, Yegengil Z (2004) Slow Senonian and fast Palaeocene-Early Eocene uplift of the granitoids in the Central Eastern Pontides, Turkey: apatite fission-track results. Tectonophysics 382:213–228. doi:10.1016/j.tecto.2004.01.001

Boztug D, Ercin AI, Kurucelik MK, Göc D, Kömür I, Iskenderoglu A (2006) Main geochemical characteristics of the composite Kaçkar batholith derived from the subduction through collision to extentional stages of Neo-Tethyan convergence system in the Eastern Pontides, Turkey. J Asian Earth Sci 27:286–302. doi:10.1016/j.jseaes.2005.03.008

Boztug D, Jonckheere R, Wagner GA, Ercin AI, Yegingil Z (2007) Titanite and zircon fission-track dating resolves successive igneous episodes in the formation of the composite Kaçkar batholith in the Turkish eastern Pontides. Int J Earth Sci 96:875–886. doi:10.1007/s00531-006-0140-4

Bruker (2005) SAINT, Version 6.0. Bruker AXS Inc., Madison

Cakir Ö, Erduran M (2004) Constraining crustal and uppermost mantle structure beneath station TBZ (Trabzon, Turkey) by receiver function and dispersion analyses. Geophys J Int 158:955–971. doi:10.1111/j.1365-246X.2004.02345.x

Cakir Ö, Erduran M, Cinar H, Yilmaztürk A (2000) Forward modelling receiver functions for crustal structure beneath station TBZ (Trabzon, Turkey). Geophys J Int 140:341–356. doi:10.1046/j.1365-246x.2000.00023.x

Cellai D, Conticelli S, Menchetti S (1994) Crystal-chemistry of clinopyroxene from potassic and ultrapotassic rocks in central Italy: implications on their genesis. Contrib Mineral Petrol 116:301–315. doi:10.1007/BF00306499

Cundari A, Salviulo G (1987) Clinopyroxenes from Somma-Vesuvius: implications of crystal chemistry and site configuration parameters for studying magma genesis. J Petrol 28:727–736

Dal Negro A, Carbonin S, Molin GM, Cundari A, Piccirillo EM (1982) Intracrystalline cation distribution in natural clinopyroxenes of tholeiitic, transitional, alkaline basaltic rocks. In: Saxena SK (ed) Advances in physical geochemistry. Springer, New York, pp 117–150

Dal Negro A, Carbonin S, Domeneghetti C, Molin GM, Cundari A, Piccirillo EM (1984) Crystal chemistry and evolution of the clinopyroxene in a suite of high pressure ultramafic nodules from the Newer Volcanics of Victoria, Australia. Contrib Mineral Petrol 86:221–229. doi:10.1007/BF00373667

Dal Negro A, Manoli S, Secco L, Piccirillo EM (1989) Megacrystic clinopyroxenes from Victoria (Australia): crystal chemical comparisons of pyroxenes from high and low pressure regimes. Eur J Mineral 1:105–121

Dinter DA (1998) Late Cenozoic extension of the Alpine collisional Orogen, northeastern Greece: origin of the north Aegean basin. Geol Soc Am Bull 110:1208–1230

Droop GTR (1987) A general equation for estimating Fe^{3+} concentrations in ferromagnesian silicates and oxides from microprobe analyses, using stoichiometric criteria. Mineral Mag 51:431–435. doi:10.1180/minmag.1987.051.361.10

Faraone D, Molin GM, Zanazzi PF (1988) Clinopyroxenes from Vulcano (Aeolian Islands, Italy): crystal chemistry and cooling history. Lithos 22:13–126. doi:10.1016/0024-4937(88)90020-5

Griffin WL, Carswell DA, Nixon PH (1979) Lower crustal granulites and eclogites from Lesotho southern Africa. In: Boyd FR, Meyer HOA (eds) The mantle sample: inclusions in Kimberlites and other Volcanics. Am Geophys Union Washington, pp 59–86

Güven IH (1993) 1/250.000 scaled geological and metallogenical map of the Eastern Black Sea Region. MTA, Trabzon (unpublished)

Hoskin PWO, Wysoczanski RJ (1998) Insitu accurate and precise lead ısotopic analysis of ultra-small analyte volumes (10–16 m^3) of solid ınorganic samples by high mass resolution secondary ıon mass spectrometry. J Anal At Spectrom 13:597–601. doi:10.1039/a801286e

Jones AP, Smith JV, Dawson B, Hansen EC (1983) Metamorphism, partial melting, and K-metasomatism of garnet-scapolite-kyanite granulite xenoliths from Lashaine, Tanzania. J Geol 91:143–165

Karsli O, Aydin F, Sadiklar MB (2002) Geothermobarometric investigation of the Zigana Granitoid, eastern Pontides, Turkey. Int Geol Rev 44:277–286. doi:10.2747/0020-6814.44.3.277

Karsli O, Aydin F, Sadiklar MB (2004a) Magma interaction recorded in plagioclase zoning in granitoid systems, Zigana Granitoid, Eastern Pontides, Turkey. Turk J Earth Sci 13:287–305

Karsli O, Aydin F, Sadiklar MB (2004b) The morphology and chemistry of K-feldspar megacrysts from İkizdere Pluton: evidence for acid and basic magma interactions in granitoid rocks, NE Turkey. Chem Erde-Geochem 64:155–170. doi:10.1016/j.chemer.2003.02.001

Karsli O, Chen B, Aydin F, Sen C (2007) Geochemical and Sr–Nd–Pb isotopic compositions of the Eocene Dölek and Sariçiçek Plutons, Eastern Turkey: implications for magma interaction in the genesis of high-K calc-alkaline granitoids in a post-collision extensional setting. Lithos 98:67–96. doi:10.1016/j.lithos.2007.03.005

Keskin M (2003) Magma generation by slab steepening and breakoff beneath a subduction-accretion complex: An alternative model for collision-related volcanism in Eastern Anatolia, Turkey. Geophys Res Lett 30(24):8046. doi:10.1029/2003GL018019

Keskin M, Genc SC, Tuysuz O (2008) Petrology and geochemistry of post-collisional Middle Eocene volcanic units in North-Central Turkey: evidence for magma generation by slab breakoff following the closure of the Northern Neotethys Ocean. Lithos 104:267–305. doi:10.1016/j.lithos.2007.12.011

Malgarotto C, Molin G, Zanazzi F (1993) Crystal chemistry of clinopyroxenes from Filicudi and Salina (Aeolian Islands, Italy). Geothermometry and barometry. Eur J Mineral 5:915–923

Molin G, Zanazzi PF (1991) Intracrystalline Fe^{2+}–Mg ordering in augite: experimental study and geothermometric application. Eur J Mineral 3:863–875

Morimoto N (1989) Nomenclature of pyroxenes. Can Mineral 27:143–156

Nazzareni S, Molin G, Peccerillo A, Zanazzi PF (1998) Structural and chemical variations in clinopyroxenes from the island of Alicudi (Aeolian Arc) and their implications for the conditions of crystallization. Eur J Mineral 10:291–300

Nazzareni S, Molin G, Peccerillo A, Zanazzi PF (2001) Volcanological implications of crystal-chemical variations in clinopyroxenes from the Aeolian Arc, Southern Tyrrhenian Sea (Italy). Bull Volcanol 63:73–82. doi:10.1007/s004450100125

Nimis P (1995) A clinopyroxene geobarometer for basaltic systems based on crystal structure modeling. Contrib Mineral Petrol 121:115–125. doi:10.1007/s004100050093

Nimis P (1998) Clinopyroxene geobarometry of pyroxenitic xenoliths from Hyblean Plateau (SE Sicily, Italy). Eur J Mineral 10:521–533

Nimis P (1999) Clinopyroxene geobarometry of magmatic rocks. Part 2. Structural geobarometers for basic to acid, tholeiitic and midly alkaline magmatic systems. Contrib Mineral Petrol 135:62–74. doi:10.1007/s004100050498

Nimis P (2000) CpxBar-Excel version program. http://dmp.unipd.it/Nimis/researche.html

Nimis P, Ulmer P (1998) Clinopyroxene geobarometer of magmatic rocks. Part 1: An expanded structural geobarometer for anhydrous and hydrous, basic and ultrabasic systems. Contrib Mineral Petrol 133:122–135. doi:10.1007/s004100050442

Nimis P, Bertolo S, Dal Negro A, Mellini M (1996) Crystal chemistry and geobarometry of clinopyroxenes in ancient and historical basic volcanic rocks Mt. Etna (Sicily, Italy). Acta Vulcanol 8:63–71

Okay AI (1989) Tectonic units and sutures in the Pontides, Northern Turkey. In: Sengör AMC (ed) Tectonic evolution of the Tethyan region. NATO ASI Ser C 259:109–116

Okay AI, Sahintürk Ö (1997) Geology of the Eastern Pontides. In: Robinson AG (ed) Regional and Petroleum Geology of the Black Sea and Surrounding Region. AAPG Memoir 68:291–311

Pasqual D, Molin GM, Zanazzi PF (1995) Crystal chemistry of Stromboli clinopyroxene: a comparison with analogues from other Aeolian Islands (Italy). Eur J Mineral 7:369–378

Princivalle F, Tirone M, Comin-Chiaramonti P (2000) Clinopyroxenes from spinel-peridotite mantle xenoliths from Nemby (Paraguay): crystal chemistry and petrological implications. Mineral Petrol 70:25–35. doi:10.1007/s007100070011

Putirka K, Johnson M, Kinzler R, Longhi J, Walker D (1996) Thermobarometry of mafic igneous rocks based on clinopyroxene-liquid equilibria, 0–30 kbar. Contrib Mineral Petrol 123:92–108. doi:10.1007/s004100050145

Putirka KD, Mikaelian H, Ryerson F, Shaw H (2003) New clinopyroxene-liquid thermobarometers for mafic, evolved, and volatile-bearing lava compositions, with applications to lavas from Tibet and the Snake River Plain, Idaho. Am Mineral 88:1542–1554

Robertson AHF (2000) Mesozoic-Tertiary tectonic-sedimentary evolution of a south Tethyan oceanic basin and its margin in southern Turkey. In: Bozkurt E, Winchester JA, Piper JDA (eds) Tectonics and magmatism in Turkey and surrounding areas. J Geol Soc Lond, Spec Publ 173:97–136

Robinson AG, Banks CJ, Rutherford MM, Hirst JPP (1995) Stratigraphic and structural development of the Eastern Pontides, Turkey. J Geol Soc Lond 152:861–872. doi:10.1144/gsjgs.152.5.0861

Sen C, Arslan M, Van A (1998) Geochemical and petrological characteristics of the Eastern Pontide Eocene (?) alkaline volcanic province, NE Turkey. Turk J Earth Sci 7:231–239

Sengör AMC, Kidd WSF (1979) Post-collisional tectonics of the Turkish-Iranian plateau and a comparison with Tibet. Tectonophysics 55:361–376

Sengör AMC, Yilmaz Y (1981) Tethyan evolution of Turkey: a plate tectonic approach. Tectonophysics 75:181–241. doi:10.1016/0040-1951(81)90275-4

Sengör AMC, Görür N, Saroglu F (1985) Strike slip faulting and related basin formation in zones of tectonic escape: Turkey as a case study. In: Biddle TR, Christie-Blick N (eds) Strike-slip deformation, basin formation and sedimentation. Int J Soc Econ Paleontol Mineral, Special Publuciation 37:227–264

Sengör AMC, Özeren S, Genc T, Zor E (2003) East Anatolian high plateau as a mantle-supported, North-south shortened domal structure. Geophys Res Lett 30(24):8045. doi:10.1029/2003GL017858

Sheldrick GM (1997) SHELXL-97, a program for crystal structure refinement. University of Göttingen, Germany

Takahashi E, Kushiro I (1983) Melting of a dry peridotite at high pressures and basalt magma genesis. Am Mineral 68:859–879

Thompson RM, Downs RT (2008) The crystal structure of diopside to 10 GPa. Am Mineral 93:177–186. doi:10.2138/am.2008.2684

Topuz G, Altherr R, Schwarz WH, Siebel W, Satir M, Dokuz A (2005) Post-collisional plutonism with adakite-like signatures: the Eocene Saraycik granodiorite (Eastern Pontides, Turkey). Contrib Mineral Petrol 150:441–455. doi:10.1007/s00410-005-0022-y

Yegingil Z, Boztug D, Er M, Oddone M, Bigazzi G (2002) Timing of neotectonic fracturing by fission-track dating of obsidian in-filling faults in the Ikizdere-Rize area, NE Black Sea region, Turkey. Terra Nova 14:169–174. doi:10.1046/j.1365-3121.2002.00407.x

Yilmaz Y, Tüysüz O, Yigitbas E, Genc SC, Sengör AMC (1997) Geology and tectonic evolution of the Pontides. In: Robinson AG (ed) Regional and Petroleum Geology of the Black Sea and Surrounding Region. AAPG Memoir 68:183–226

Yilmaz A, Adamia S, Chabukiani A, Chkhotua T, Erdogan K, Tuzcu S, Karabiyikoglu M (2000) Structural correlation of the southern Transcaucasus (Georgia)-eastern Pontides (Turkey). In: Bozkurt E, Winchester JA, Piper JDA (eds) Tectonics and magmatism in Turkey and surrounding area. Geol Soc Lond Spec Pub 173:171–182